Clim. Past, 11, 187–202, 2015
www.clim-past.net/11/187/2015/
doi:10.5194/cp-11-187-2015

Nutrient utilisation and weathering inputs in the Peruvian upwelling region since the Little Ice Age

C. Ehlert[1,*] **9.9626 Tf 9.963t110(Ehlert)Grasseg 0 G/F66 7.5716 Tf 39.292 44.283Td [(1)]TJ0 g 0 G [(,)]T9626 Tf 9.963 -4.284 Td [(**

(16 S; Reuter et al., 2009). On the one hand this caused growth and extension of the Andean glaciers (Vuille et al., 2008) and on the other it enabled human settlements in the presently hyperarid southern Peruvian Andes (Unkel et al., 2007). In the upwelling areas off Peru and the western South American shelf regions, the main consequence of these climatic conditions during the LIA was a deepening of the nutricline and a strongly diminished biological productivity (Vargas et al., 2007; Sifeddine et al., 2008; Valdés et al., 2008; Gutiérrez et al., 2009).

Sediment cores from the Peruvian shelf covering the period of time from the LIA until present indicate that the marine realm was characterised by an abrupt biogeochemical regime shift towards modern conditions at the end of the LIA due to the northward movement of the ITCZ and an expansion of the SPSH. While low productivity and a more oxygenated water column prevailed during the LIA, markedly increased biological productivity and pronounced oxygen depletion over wide areas of the shelf have characterised the system since the end of the LIA (Vargas et al., 2007; Sifeddine et al., 2008; Gutiérrez et al., 2009; Salvatteci et al., 2014a).

In this study the stable silicon isotope composition of sedimentary diatoms ($^{30}Si_{opal}$/ covering the period of time from the LIA to the present is analysed. The main goal is the reconstruction of the factors controlling the dynamics of nutrient cycling together with oxygen in the Peruvian upwelling, in particular a comparison between the $^{30}Si_{opal}$ and the stable nitrogen isotope composition ($^{15}N_{sed}$/ of sedimentary organic matter. Both $^{30}Si_{opal}$ and $^{15}N_{sed}$ provide information about utilisation of silicic acid ($Si(OH)_4$/ and nitrate (NO_3 / during primary productivity, e.g. during the formation of diatom frustules and associated organic matter, respectively (Altabet and Francois, 1994; De La Rocha et al., 1997). Diatoms preferentially incorporate the lighter isotopes from the dissolved $Si(OH)_4$ and NO_3 pools, leaving the residual dissolved nutrients enriched in the heavier isotopes (Wada and Hattori, 1978; Altabet et al., 1991; De La Rocha et al., 1997). Si isotope fractionation is mainly controlled by the utilisation of $Si(OH)_4$ in surface waters by biota (diatoms) (e.g. De La Rocha et al., 1998; Brzezinski et al., 2002; Egan et al., 2012). The ^{15}N of NO_3 is partly controlled by NO_3 utilisation of marine organisms but is also affected by N-loss processes in the water column (denitrification, anammox) (Codispoti et al., 2001; Dalsgaard et al., 2003), resulting in a marked enrichment of the upwelling source waters in the heavier $^{15}NO_3$ (Liu and Kaplan, 1989; Lam et al., 2009; given that it is currently not possible to distinguish between different N-loss processes from the sediments, we will use the term denitrification for simplicity). Consequently, sedimentary $^{15}N_{sed}$ records from areas dominated by oxygen-depleted waters such as the shelf region off Peru are usually interpreted to directly reflect changes in the intensity of subsurface NO_3 loss and the extent and strength of oxygen depletion (e.g. De Pol-Holz et al., 2007, 2009; Agnihotri et al., 2008; Gutiérrez et al., 2009), whereas the effect of NO_3 utilisation on the preserved $^{15}N_{sed}$ is often neglected. Comparison of both isotope systems can therefore provide information about the degree of utilisation of NO_3 and $Si(OH)_4$ versus the influence of NO_3 loss processes. Increasing nutrient utilisation should result in a consistent increase in both $^{30}Si_{opal}$ and $^{15}N_{sed}$. In contrast, a change in NO_3 reduction due to varying oxygen depletion in the water column would affect only the $^{15}N_{sed}$, leaving the $^{30}Si_{opal}$ unaffected.

The main forces driving surface productivity and subsurface oxygenation off Peru at centennial timescales during the past two millennia have been changes in the strength of the Walker circulation and in the expansion/contraction of the SPSH (Gutierrez et al., 2009; Salvatteci et al., 2014a). Therefore, the radiogenic isotope compositions of neodymium (ε_{Nd}/ and strontium ($^{87}Sr/^{86}Sr$) of the authigenic ferromanganese (Fe-Mn) oxyhydroxide coatings of the sedimentary particles, which are expected to record the radiogenic isotope compositions of past bottom waters, as well as of the detrital fraction of the sediment were examined. These proxy data provide information about changes in (surface ocean) circulation and transport processes, provenance of the sediments, and input mechanisms of terrigenous material as a function of changes in precipitation on land during the transition from wetter LIA conditions to drier modern conditions. Weathering of continental source rocks delivers lithogenic particles of different origin and age to the shelf, which have distinct radiogenic isotope signatures ($\varepsilon_{Nd\ detritus}$, $^{87}Sr/^{86}Sr_{detritus}$/ that can be used to trace their source areas (Goldstein et al., 1984). Central Peruvian Andean rocks have more radiogenic ε_{Nd} signatures whereas southern Peruvian rocks are characterised by less radiogenic ε_{Nd} signatures (Sarbas and Nohl, 2009), which is also reflected in the sediments along the shelf (Ehlert et al., 2013). Changes in detrital material input and transport pathways are generally closely related to climatic changes causing variations in the supply from the respective source areas (e.g. Grousset et al., 1988). It should therefore be possible to detect the transition from wetter LIA conditions with higher local input from central Peru via rivers due to higher precipitation rates towards the drier presently prevailing conditions with an increased influence of aeolian material transport from further south in the Atacama Desert (Molina-Cruz, 1977) and deposition along the shelf after the LIA.

2 Material and methods

2.1 Core locations and age models

For the reconstruction of surface water $Si(OH)_4$ utilisation and terrestrial material input and transport for the period of time between the LIA and present, two sediment cores with high sedimentation rates were analysed. Box core B0405-6 was recovered from the upper continental slope off Pisco at

Table 1. Downcore records of core M771-470 for $^{30}Si_{opal}$ (‰); bSi content (wt %); and $^{143}Nd/^{144}Nd$, ε_{Nd} and $^{87}Sr/^{86}Sr$ of detrital material. $2_{(sd)}$ represents the external reproducibilities of repeated sample (Si) and standard (Nd, Sr) measurements.

Depth (cm)	$^{30}Si_{opal}$ (‰)	$2_{(sd)}$	bSi (wt %)	$^{143}Nd/^{144}Nd_{detritus}$	$\varepsilon_{Nd\ detritus}$	$2_{(sd)}$	$^{87}Sr/^{86}Sr_{detritus}$	$2_{(sd)}$
0.5	1.03	0.15	18.8	–	–	–	–	–
1.5	–	–	18.6	–	–	–	–	–
2.5	–	–	22.2	–	–	–	–	–
3.5	0.93	0.08	16.9	0.512369	5.2	0.3	0.709315	1.5e-05
4.5	–	–	16.3	–	–	–	–	–
5.5	–	–	17.2	0.512381	5.0	0.3	0.709356	1.5e-05
7	–	–	19.5	–	–	–	–	–
9	0.96	0.09	19.8	0.512398	4.7	0.3	0.708822	1.5e-05
11	–	–	18.8	–	–	–	–	–
13	–	–	15.9	–	–	–	–	–
15	–	–	–	0.512383	5.0	0.3	0.708737	1.5e-05
16	0.96	0.07	19.3	–	–	–	–	–
19	–	–	–	0.512386	4.9	0.3	0.708552	1.5e-05
20	1.05	0.10	18.9	0.512410	4.5	0.3	0.708412	8.0e-06
23	–	–	–	0.512393	4.8	0.3	0.708720	1.5e-05
24	1.15	0.13	26.9	–	–	–	–	–
26	–	–	–	0.512387	4.9	0.3	0.707482	8.0e-06
27	–	–	–	0.512397	4.7	0.3	0.707555	1.5e-05
28	1.00	0.14	14.0	–	–	–	–	–
29	–	-	–	0.512452	3.6	0.3	0.706549	1.5e-05
32	0.55	0.17	10.1	0.512442	3.8	0.3	0.706763	1.5e-05
32	–	–	–	0.512445	3.8	0.3	0.706469	8.0e-06
36	1.10	0.15	14.4	0.512419	4.3	0.3	0.706767	8.0e-06
40	0.79	0.11	12.3	0.512408	4.5	0.3	0.706964	8.0e-06
44	0.91	0.18	15.0	0.512421	4.2	0.3	0.707057	8.0e-06
48	0.75	0.05	–	0.512395	4.7	0.3	0.707816	8.0e-06

Table 2. Downcore records of core B0405-6 for $^{30}Si_{opal}$ (‰); bSi content (wt %); and $^{143}Nd/^{144}Nd$, ε_{Nd} and $^{87}Sr/^{86}Sr$ of detrital material. $2_{(sd)}$ represents the external reproducibilities of repeated sample (Si) and standard (Nd, Sr) measurements.

Year AD	$^{30}Si_{opal}$ (‰)	$2_{(sd)}$	bSi (wt %)	$^{143}Nd/^{144}Nd_{detritus}$	$\varepsilon_{Nd\ detritus}$	$2_{(sd)}$	$^{87}Sr/^{86}Sr_{detritus}$	$2_{(sd)}$
1950	0.91	0.15	21.7	0.512507	2.6	0.1	0.708372	8.0e-06
1925	0.83	0.15	21.0	0.512460	3.5	0.3	0.707923	8.0e-06
1903	0.62	0.10	18.9	0.512487	2.9	0.3	0.707715	8.0e-06
1857	1.02	0.16	34.4	0.512471	3.3	0.3	0.707829	8.0e-06
1857	1.22	0.14	37.7	0.512481	3.1	0.1	0.707736	8.0e-06
1818	0.56	0.15	12.6	0.512468	3.3	0.3	0.707702	8.0e-06
1793	0.82	0.14	15.8	0.512446	3.7	0.3	0.7074nt21	

Figure 2. Downcore records for core M771-470 (upper panel) and core B0405-6 (lower panel). The blue and yellow shadings indicate the age range of the LIA and the transitional period, respectively. **(a, e)** bSi concentration (black squares), **(a, e, i)** total N concentration (dashed blue curve), **(e)** diatom accumulation rate (grey bars) (Gutiérrez et al., 2009), **(b, f)** $^{30}Si_{opal}$ (red squares), **(f)** bulk $^{15}N_{sed}$ (grey curve) (Gutiérrez et al., 2009), **(c, g)** $\varepsilon_{Nd\ detritus}$ (black squares), **(d, h)** $^{87}Sr = {}^{86}Sr_{detritus}$ (grey diamonds; x axis is inverted), **(d)** sediment porosity (grey curve). Error bars represent 2 $_{(sd)}$ external reproducibilities of repeated standard or sample measurements. For comparison, **(i)** shows the total N content and $^{15}N_{sed}$ of core B0405-13 (Gutiérrez et al., 2009).

and Sr in the leachates and in the completely dissolved detrital sediment fraction followed previously published procedures for Nd (Cohen et al., 1988) and Sr (Horwitz et al., 1992) applying ion exchange chromatography for separation of Rb/Sr from the rare earth elements (REEs) (0.8 mL AG50W-X12 resin, mesh 200–400) followed by separation of Sr from Rb (50 µL Sr-Spec resin, mesh 50–100), and separation of Nd from the other REEs (2 mL Eichrom Ln-Spec resin, mesh 50–100). All radiogenic isotope measurements were performed on the Nu Plasma HR MC-ICPMS (Nu Instruments) at GEOMAR. Measured Nd isotope compositions were corrected for instrumental mass bias using a $^{146}Nd = {}^{144}Nd$ ratio of 0.7219 and were normalised to the accepted $^{143}Nd = {}^{144}Nd$ literature value of 0.512115 of the JNdi-1 standard (Tanaka et al., 2000). All values are given as ε_{Nd}, which corresponds to the measured $^{143}Nd = {}^{144}Nd$, normalised to the chondritic uniform reservoir (CHUR) (0.512638), multiplied by 10 000. The external reproducibility was estimated via repeated measurements of the JNdi-1 standard and was always better than 20 ppm (2 $_{(sd)}$, Tables 1, 2). Measured $^{87}Sr = {}^{86}Sr$ ratios were corrected for instrumental mass bias using $^{88}Sr = {}^{86}Sr$ D 8.3752 and were normalised to the accepted value for NIST SRM987 of 0.710245. The 2 $_{(sd)}$ external reproducibility of repeated standard measurements was always better than 36 ppm (2 $_{(sd)}$, Tables 1, 2). Procedural Nd and Sr blanks for leachates and total dissolutions of the detrital material were 83 pg and 2.1 ng, respectively, and thus negligible compared to the concentrations of the samples.

3 Results

3.1 Core M771-470 (Callao)

Sediment core M771-470, from a location at 11 S 145 m water depth, is characterised by bSi concentrations between 10.1 and 26.9 % and total N contents between 0.5 and 1.1 % (Fig. 2a, Table 1), whereby the lowest values occurred just prior to the end of the LIA. The maximum bSi concentrations were found during the transition period. In contrast, the highest nitrogen (N) content occurred later in the youngest part of the record. The $^{30}Si_{opal}$ varied between C0.6 and

C1.1 ‰ (Fig. 2b) and followed bSi concentrations with the maximum and minimum isotope values corresponding to the

Pisco show the characteristic coeval pronounced increase in bSi and total N content (Fig. 2a, e) and C_{org} concentration (not shown here) after the end of the LIA and during the transition period. Therefore, three time periods that show distinct differences in productivity and nutrient utilisation have been identified from our records and will be discussed in the following: the LIA, the transition period from the LIA to mod-

a) b) c)

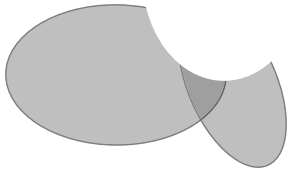

Figure 3.

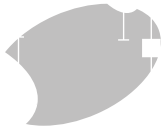

B0405-6:
LIA
transition period
modern

Figure 4. Relationship between $^{15}N_{sed}$ versus $^{30}Si_{opal}$ for **(a)** surface sediments and **(b)** downcore data from core B0405-6. The crosses in **(a)** indicate ^{30}Si data obtained from hand-picked diatoms, which reflect a different growth season than bulk $^{30}Si_{opal}$ and which are influenced by stronger $Si(OH)_4$ limitation (higher ^{30}Si) (Ehlert et al., 2012). The solid lines reflect theoretical utilisation (assuming 1 : 1 utilisation of $Si(OH)_4$ and NO_3 by the diatoms) and the dashed lines mark the theoretically expected line for denitrification, which represent the expected signal preserved in the sediments, based on present-day measurements: ^{30}Si source signature and enrichment factor $\varepsilon_{diatom\ Si.OH/4}$ are always −1.5 ‰ (Ehlert et al., 2012) and −1.1 ‰ (De La Rocha et al., 1997), respectively. $^{15}N_{sed}$ source signature and $\varepsilon_{organic\ NO_3}$ vary with latitude (Mollier-Vogel et al., 2012); in the north at 3.6° S, source signature and ε are −5.7 and −3.7 ‰ (red curves); along the central shelf at 13.7° S, source signature and ε are −8.9 and −4.8 ‰ (green curves); and in the south at 17° S, source signature and ε were measured to be −14.5 and −5.7 ‰ (blue curves), respectively. The samples are colour-coded according to their location on the shelf and relative to the NO_3 utilisation/NO_3 loss that they experienced. Data points that plot above the utilisation curves reflect predominant $Si(OH)_4$ limitation, whereas data points below record stronger NO_3 limitation. The isotopic enrichment during denitrification was always set to be −20 ‰. For the downcore data **(b)** two different assumed source signatures are displayed: −9 ‰ (green lines, corresponding to the modern conditions along the central shelf region in **a**) and −6 ‰ (grey lines). Data points are colour-coded according to the respective time periods (black: LIA; white: transition period; grey: modern). Error bars represent 2 $_{(sd)}$ external reproducibilities.

depletion. Overall, however, the utilisation signal appears to have dominated both the Si and N isotope records.

If, however, the $^{15}N_{sed}$ is dominated by utilisation it is interesting that $^{15}N_{sed}$ and proxies for sediment redox conditions (e.g. molybdenum concentrations) in the cores (both B0405-6 and B0405-13) are strongly coupled throughout the record (Sifeddine et al., 2008; Gutiérrez et al., 2009). One direct interpretation could be that the diatom blooms, and subsequently the degradation of the organic matter, strongly control the oxygen availability in the sediments after sedimentation and burial. Therefore, increased diatom productivity and higher $Si(OH)_4$ and NO_3 utilisation would result in an increase in $^{15}N_{sed}$. At the same time, more oxygen is consumed during degradation of the organic matter in the sediments, causing more reducing conditions in the sediments. Consequently, a change in the subsurface water column structure, e.g. enhanced re-supply of oxygen via ocean currents, may not be reflected in the $^{15}N_{sed}$ record.

4.1.4 Modelling the surface water utilisation

Following the above considerations we will try to quantify past utilisation based on our data. The theoretical relationship between the degree of surface water nutrient utilisation and the stable isotope composition of Si and N can be described assuming either Rayleigh-type (single input followed by no additional nutrients newly supplied to a particular parcel of water followed by fractional loss as a function of production and export) or steady-state (continuous supply and partial consumption of nutrients causing a dynamic equilibrium of the dissolved nutrient concentration and the product) fractionation behaviour (Fig. 5) (Mariotti et al., 1981). The lighter isotopes are preferentially incorporated into the diatom frustules and the organic matter, respectively, leaving the dissolved fraction enriched in the heavier isotopes (Wada and Hattori, 1978; Altabet et al., 1991; De La Rocha et al., 1997). The fractionation between ^{30}Si in seawater and ^{30}Si in the produced diatom opal has generally been assumed to be −1.1 ‰ (De La Rocha et al., 1997), whereas between

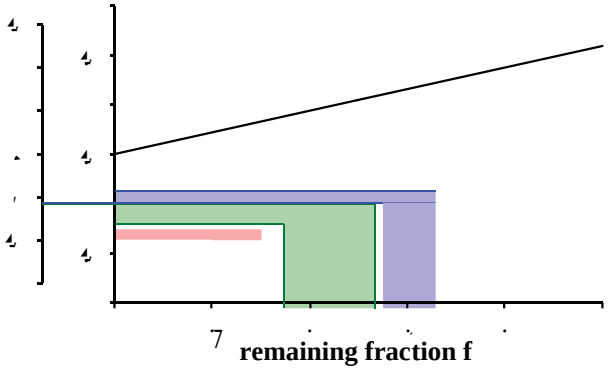
remaining fraction f

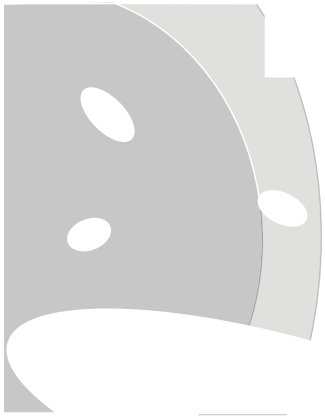

Figure 6. $\varepsilon_{Nd\ detritus}$ versus $^{87}Sr/^{86}Sr_{detritus}$ for core M771-470 (red diamonds) and B0405-6 (blue squares). Error bars represent 2 (sd) external reproducibilities. The green dots are data obtained from surface sediment samples at different sites on the Peruvian shelf. The grey shadings indicate potential sources and provenance end members of the detrital material.

This suggests that the nutrient concentrations in the upwelled subsurface source waters must have been lower during the LIA than they are today. During the LIA, large-scale circulation changes, i.e. a weak Walker circulation and a contraction of the SPSH (Conroy et al., 2008; Lamy et al., 2001), caused permanent El Niño-like conditions along the Peruvian upwelling system. During such conditions, the alongshore winds weakened and caused a deepening of the thermo-, oxy- and nutricline, and therefore a reduction of vertical pumping of nutrient-rich and oxygen-depleted subsurface waters off Peru. Such a reduced nutrient supply to the euphotic zone from subsurface waters resulted in an increase in nutrient deficit in surface waters and decreased biological productivity. Enhanced water column oxygenation and lower organic matter flux led to decreased organic matter preservation in the sediments.

4.1.5 Factors influencing the reconstruction of the utilisation signals

There are two main factors that can influence the reconstruction of nutrient utilisation in the past: (1) a change in the dominating diatom assemblages has to be considered, and (2) the interpretation strongly depends on the assumptions for the environmental conditions, e.g. source water signature and isotope enrichment during utilisation.

Varying upwelling and nutrient supply conditions also cause changes in the dominating diatom assemblages. Recent results from culturing experiments suggest species-dependent enrichment factors for diatom ^{30}Si (0.5 to 2.1 ‰ ; Sutton et al., 2013) and also diatom frustule-bound ^{15}N (1.9 to 11.2 ‰; Horn et al., 2011). This raises the question of whether a change in diatom assemblages may have been the cause of the observed downcore $^{30}Si_{opal}$ and, to a lesser extent, the bulk $^{15}N_{sed}$ variations. The quasi-monospecific diatom layers from the transition period AD 1820–1870 consist mainly of *Skeletonema* spp., similar to the a
1.0 ‰, mined (De la Rocha et al., 1997 also contain abundant upwelling- *Thalassionema nitzschioides* and et al., 2007), whereby *Chaetocero* Southern Ocean, has been shown of 2.1 ‰ (Sutton et al., 2013). $^{30}Si_{sed}$

The assumed source water $^{30}Si_{Si.OH/4}$ and $^{15}N_{NO_3}$ values of −1.5 and −9 ‰ (Figs. 5, 6), respectively, were measured in the present-day subsurface waters under strong upwelling conditions during which high amounts of nutrients are supplied to the euphotic zone (Ehlert et al., 2012; Mollier-Vogel et al., 2012). Under strong upwelling conditions the bottom waters on the shallow shelf are today dominated by

After the end of the LIA the region experienced a northward displacement of the ITCZ and the northern rim of the

Acknowledgements. This work is a contribution of Sonderforschungsbereich 754 "Climate–Biogeochemistry Interactions in the Tropical Ocean" (www.sfb754.de), which is supported by the Deutsche Forschungsgemeinschaft. We acknowledge the help of Jutta Heinze in the laboratory of GEOMAR for the biogenic opal concentration measurements. We thank Ulrike Lomnitz and Klaus Wallmann for their help with the ^{210}Pb dating and the establishment of the age model of core M771-470.

The service charges for this open access publication have been covered by a Research Centre of the Helmholtz Association.

core top calibration, Geochim. Cosmochim. Ac., 96, 174–192, 2012.

Ehlert, C., Grasse, P., Mollier-Vogel, E., Böschen, T., Franz, J., De Souza, G. F., Reynolds, B. C., Stramma, L., and Frank, M.: Factors controlling the silicon isotope distribution in waters and surface sediments of the Peruvian coastal upwelling, Geochim. Cosmochim. Ac., 99, 128–145, 2012.

Ehlert, C., Grasse, P., and Frank, M.: Changes in silicate utilisation and upwelling intensity off Peru since the Last Glacial Maximum – insights from silicon and neodymium isotopes, Quaternary Sci. Rev., 72, 18–35, 2013.

Estrada, M. and Blasco, D.: Phytoplankton assemblages in coastal upwelling areas, in: Simposio Internacional Sobre Las Areas de Afloramiento Mas Importantes del Oeste Africano (Cabo Blanco y Benguela), edited by: Bas, C., Margalef, R., and Rubies, P., Barcelona, Instituto de Investigaciones Pesqueras, 379–402, 1985.

Georg, R. B., Reynolds, B. C., Frank, M., and Halliday, A. N.: New sampleandFrtechni80(smple)-f23623(Frthample)-deland3heFrSi-23(3h-220.959 Td [(bies,)-280)-3ic-239-2083(Intand)s-239-2usreas,38(ImC9(a-ICPM

Georg,B.S.-23(Frnd)-2m75(O'Nnd)sR.-23(FrKd)-2m75(u-)]TJ75(H99(lteochim(Fr281(Bar]TJ75(J)5(yt75(A-23(FrSm -10Nd-10.959 Td [(sample)-37-2

Müller, P. J. and Schneider, R. R.: An automated leaching method for the determination of opal in sediments and particulate matter, Deep-Sea Res. Pt. I, 40, 425–444, 1993.

Piepgras, D. J. and Wasserburg, G. J.: Isotopic Composition of Neodymium in Waters from the Drake Passage, Science, 217, 207–214, 1982.

Rabatel, A., Francou, B., Jomelli, V., Naveau, P., and Grancher, D.: A chronology of the Little Ice Age in the tropical Andes of 9hr/]TJ 0 -10.959 Td [(2li)25(vi)-2516((16]TJ /F6 T7.571 Tf 529.607 3.255Td [(2]TJ /F